Metallophilic and Inter-Ligand Interactions in Diargentous Compounds Bound by a Geometrically Flexible Macrocycle

Qiuran Wang, Michael R. Gau, Brian C. Manor, Patrick J. Carroll, and Neil C. Tomson*

Dr. Q. Wang, Dr. M. R. Gau, Dr. B. C. Manor, Dr. P. J. Carroll, Prof. N. C. Tomson

Roy and Diana Vagelos Laboratories, Department of Chemistry

University of Pennsylvania

231 South 34th Street, Philadelphia, Pennsylvania, 19104, USA

E-mail: tomson@upenn.edu

URL: http://tomsongroup.chem.upenn.edu

Supporting information for this article is given via a link at the end of the document.

Abstract: A series of mono- and di-nuclear Ag(I) complexes supported by a flexible macrocyclic ligand are reported. The geometric flexibility of the ligand was found to allow for a range of Ag-Ag interactions in the disilver complexes, depending on the identities of both the ancillary ligand and the counterion. Studies of the solution-phase dynamic exchange processes for these latter complexes found rapid interconversion through a mechanism that retained the multi-nuclearity. Quantum Theory of Atoms in Molecules (QTAIM) and Independent Gradient Model based Hirshfeld partition (IGMH) analyses are used to evaluate the d¹⁰-d¹⁰ interactions between silver centers in the various geometries observed for the solid-state structures of these complexes, revealing nearly identical Ag-Ag interactions, regardless of the relative geometries of the Ag centers. Instead, a weak, but non-negligible, inter-ligand interaction between two isocyanide units may contribute to the folded-ligand geometry observed in the solid state.

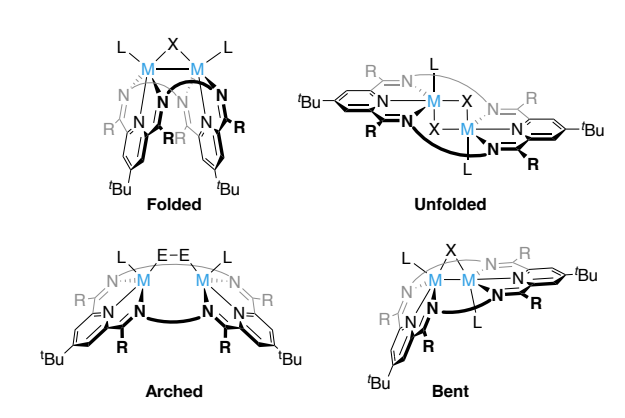
Introduction

Multinuclear Ag(I) complexes have been used for a wide range of applications, including luminescent materials, [1] antibiotics, [2] and catalysts. [3] The closed-shell interactions between such d10 metal centers are more complex than they would appear at first glance. As such, their metallophilic [4] nature has received a significant amount of attention from experimentalists and theoreticians in attempts to develop an understanding of the weak interactions between these large metal ions. [5]

Much experimental work studying metallophilic interactions has been conducted, especially with respect to the formation of short and strong interactions.^[6] The physical properties of these complexes have been used to support computational investigations into the nature of closed-shell metallophilic interactions, with several models having been developed. Hoffmann and co-workers first proposed that the metal (n+1)s and (n+1)p manifolds hybridize with the valence nd set to create an overall net bonding interaction between d¹⁰ centers.^[5a] Pyykkö and co-workers studied the metallophilic interactions between two d¹⁰ metal centers in a series of [XM(PR₃)]₂ dimers (X = H, F, Cl, Br, I, CH₃ and CCH; M = Cu, Ag, Au; PR₃ = PH₃ and PMe₃) and concluded that metallophilic interactions result from electron correlation that is strengthened by relativistic effects.^[5b, 7] More recently, Che and co-workers proposed *repulsive* metal-metal

interactions in a series of di-Ag(I) and di-Au(I) complexes and emphasized the importance of attractive ligand-ligand dispersion and electrostatic interactions^[5c, 5d] to counterbalance the repulsive M–M interactions.^[5e] It can be seen from the above examples that despite the effort devoted to the deconvolution of metallophilic interactions, this topic still remains controversial.

Ag(I)···Ag(I) metallophilic interactions are among the most studied and reported examples of metallophilic interactions. Topics of interest in Ag(I)···Ag(I) metallophilic interactions include their effects on molecular structures, [4, 8] supramolecular assemblies, [9] photophysical and biological properties, [10] and the electronic properties of these interactions.^[5, 11] We have recently made use of pyridyldiimine-derived macrocyclic ligands to support bimetallic complexes of first-row transition metals^[12] and studied the effect of ligand folding on metal-metal interactions on a diiron platform.[12e] We reasoned that the range of geometries available to this ligand class would allow for the investigation of metal-metal interactions between d10 coinage metal centers within a number of closely related coordination environments (Scheme 1). In so doing, we sought to study metallophilic interactions between d10 metals and examine the extent to which these interactions may contribute to the coordination chemistry within a ligand system that has shown the unusual ability to adopt such a broad range of geometries. The synthesis and characterization of mono- and diargentous complexes are presented below, along with Quantum Theory of Atoms in Molecules (QTAIM) and Independent Gradient Model based Hirshfeld partition (IGMH) methods to investigate the intramolecular interactions between the two silver-containing units.



Scheme 1. Various geometries of pyridyldiimine-based macrocyclic ligands that have been shown to support dinuclear complexes.

Results and Discussion

Synthesis of a Polymeric Ag Complex

A convenient entry into the present chemistry was found by performing cation metathesis with a Group 2 metal salt of the aldimine-based ³PDAl₂ ligand, which consists of pyridyldialdimine fragments connected through their aldimine $(CH_2)_3$ linkers.[12g],[13] nitrogens bv The species $\{[(^3PDAI_2)Ag_2(NCMe)][OTf]_2\}_n (\{[Ag_2(NCMe)][OTf]_2\}_n, Scheme 2)$ was synthesized in good yield as an off-white solid by treatment of the previously reported [(3PDAI2)Sr][OTf]2 salt with 2.0 equiv. of AgNO₃.

Scheme 2. Synthesis of {[Ag2(NCMe)][OTf]2}n.

A crystallographic analysis of {[Ag2(NCMe)][OTf]2}n revealed a silver chain in the crystal lattice of this complex (Fig. 1) that is reminiscent of previously reported terpyridine- or bipyridinesupported silver complexes.^[14] The silver chain is almost linear, as indicated by the two unique Ag-Ag-Ag angles (∠Ag2-Ag1- $Ag2' = 170.749(8)^{\circ}$, $\angle Ag1 - Ag2' - Ag1' = 180^{\circ}$), and consists of two different Ag atoms. Ag1 is bound within the pocket of a folded, pseudo-C2-symmetric ³PDAl₂ macrocyclic ligand. This binding involves the coordination of two N_{py} atoms (N2, avg. $d(Ag1-N_{py}) = 2.521 \text{ Å})$, two N_{ald} atoms (N3, avg. $d(Ag1-N_{ald}) =$ 2.493 Å), and an acetonitrile molecule ($d(Ag1-N_{MeCN}) = 2.326(3)$ Å), forming a [Ag(NCMe)]* unit (Fig. 1a). Ag2 (and Ag2') lies in a planar coordination environment (Σ∠Ag1-Ag2-N = 360°)[15] and is coordinated to two N_{ald} atoms (N1, avg. $d(Ag2-N_{ald}) = 2.145 \text{ Å}$) on different ³PDAI₂ ligands, thus forming a "bridge" between two [Ag(NCMe)]* units. The [Ag(NCMe)]* units in the silver chain are in a staggered conformation, with a 180° rotation relative to each nearest neighbor in order to reduce steric repulsion (Fig. 1b). The distance between Ag1 and Ag2 is 2.99696(15) Å, which is similar to the Ag-Ag distances reported in other polymeric Ag chains coordinated with multidentate ligands (ca. 3.0 Å).[8a, 14b, 16] The polymeric structure of $\{[Ag_2(NCMe)][OTf]_2\}_n$ might be supported by the ability of the ³PDAl₂ ligand to simultaneously coordinate to two different Ag centers, but the Ag-Ag distances are significantly shorter than twice the van der Waals radius of Ag (5.06 Å),[17] indicating the presence of metallophilic interactions between the Ag atoms. $^{[4,\ 8a,\ 10b,\ 11a]}$ Lastly, the Δ_{expt} value, an empirical metric for the extent of PD(A)I reduction, $^{[18]}$ of 0.174 Å reveals a (3PDAI₂)⁰ physical oxidation state of the macrocyclic ligand (Table 1), consistent with the presence of Ag(I) ions along the chain.

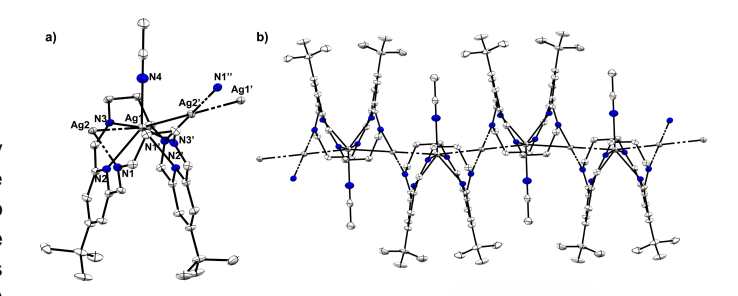


Figure 1. a) Crystal structure of the [Ag₂(NCMe)]⁺ unit, along with the positions of Ag2', Ag1' and N1", to illustrate the "bridging" mode of Ag2'; b) illustration of the 1D chain of [Ag₂(NCMe)]²⁺ monomers in the crystal of {[Ag₂(NCMe)][OTf]₂}_n. Thermal ellipsoids at the 50% probability level; hydrogen atoms and triflate ions were omitted for clarity.

Table 1. Averaged crystallographic metrics of {[Ag2(NCMe)][OTf]2}n.

	Bond lengths	$\{[Ag_2(NCMe)][OTf]_2\}_n$
	d(Ag1-Ag2) / Å	2.99696(15)
	d(Ag1-N2) / Å	2.5214
	d(Ag1–N3) / Å	2.4928(15)
	d(Ag1-N4) / Å	2.326(3)
	d(Ag2–N1) / Å	2.1447
\	d(N2-C _{ipso}) / Å	1.344
	d(C _{ipso} -C _{ald}) / Å	1.481
	d(C _{ald} -N1) / Å	1.273(2)
	d(C _{ald} -N3) / Å	1.265(2)
	Δ _{expt} / Å	0.174

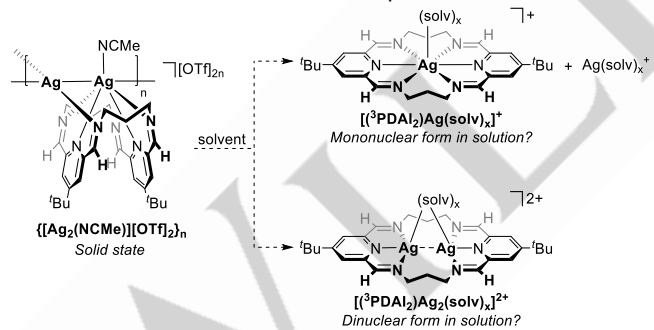
In sharp contrast to the approximate C2 symmetry of the [Ag(NCMe)]⁺ unit in the solid state, ¹H NMR spectroscopic revealed that the macrocyclic ligand $\{[Ag_2(NCMe)][OTf]_2\}_n$ exhibits D_{2h} -symmetry in acetonitrile at room temperature. We reasoned that for this to happen, 1) the silver chain must rupture in solution and 2) a fast dynamic exchange in the conformation of the ligand must occur. An NMR DOSY experiment of a mixture of [(3PDAI₂)Sr][OTf]₂, [(2PDAl2)Sr][OTf]2[12g] (an analog of the previous complex, containing ethylene linkers instead of the propylene linkers in ³PDAl₂), and $\{[Ag_2(NCMe)][OTf]_2\}_n$ in methanol- d_4 at room temperature revealed that these three complexes share similar diffusion constants of ca. $D = 2 \times 10^{-6}$ cm²/s (Table 2, Fig. S5), suggesting that {[Ag2(NCMe)][OTf]2}n exists in a monomeric form in solution at room temperature, despite the apparent presence of Ag...Ag metallophilic interactions in the solid state. Variable-¹H NMR temperature spectroscopic studies ${[Ag_2(NCMe)][OTf]_2}_n$ in CD₃CN (Fig. S6) revealed the broadening of the ligand's pyridyl hydrogen signals (7.76 ppm) and propylene linker hydrogen signals (3.94 ppm and 2.41 ppm) as the temperature of the system was decreased, suggesting that a dynamic process involving both ligand conformational exchange

and a change in the coordination mode of the PDAI unit to the Ag centers in solution may be occurring. However, at 235 K, the 1H NMR spectrum still exhibited $D_{2\rm h}$ symmetry, indicating that the activation energy of this exchange process is very low. $\{[Ag_2(NCMe)][OTf]_2\}_n$ is insoluble in THF and reacts with dichloromethane to form a white precipitate, which inhibited further investigation into this dynamic exchange process.

Table 2. Diffusion constants of $\{[Ag_2(NCMe)][OTf]_2\}_n$, $[(^3PDAI_2)Sr][OTf]_2$ and $[(^2PDAI_2)Sr][OTf]_2$ in methanol- d_4 at room temperature, as determined by an NMR DOSY experiment.

	D / (10 ⁻⁶ cm ² /s)
{[Ag ₂ (NCMe)][OTf] ₂ } _n	2.1±0.2
[(3PDAI ₂)Sr][OTf] ₂	2.0±0.2
[(2PDAI2)Sr][OTf]2	2.0±0.2

The NMR DOSY experiment on $\{[Ag_2(NCMe)][OTf]_2\}_n$ revealed its monomeric nature in solution, but information about the nuclearity of the multimetallic center in the ³PDAI₂ ligand scaffold remained unknown. We reasoned that the monomeric unit of $\{[Ag_2(NCMe)][OTf]_2\}_n$ in solution could either be mononuclear, such that both a $[(^3PDAI_2)Ag(solv)_x]^+$ species $(\mbox{Ag(solv)}_{\mbox{\tiny X}}^{\mbox{\tiny +}} \mbox{ coordinated by } ^{\mbox{\tiny 3}}\mbox{PDAl}_{\mbox{\tiny 2}})$ and a macrocycle-free Ag(solv)_x⁺ species co-exist in solution (solv = coordinated solvent dinuclear, molecule). or consisting of [(3PDAl₂)Ag₂(solv)_x]²⁺ species in solution (Scheme 3). We next attempted the isolation of mononuclear and dinuclear silver complexes using{[Ag2(NCMe)][OTf]2}n as a starting material. As described below, it was found that $\{[Ag_2(NCMe)][OTf]_2\}_n$ is indeed able to serve as the synthon for a wide variety of mononuclear and dinuclear silver complexes.



Scheme 3. Two possible forms of the monomeric unit of $\{[Ag_2(NCMe)][OTf]_2\}_n$ in solution. $(solv)_x$ represents coordinated solvent molecules.

Synthesis of Mononuclear Ag Complexes

Treatment of **{[Ag₂(NCMe)][OTf]₂}_n** with 1.0 equiv. of NaBPh₄ in THF resulted in a golden yellow solution with the concomitant formation of a white precipitate. Upon layering the solution with n-hexane at room temperature, yellow bar-like crystals were formed in moderate yield (Scheme 4). Analysis by single-crystal X-ray diffraction revealed a mono-silver species, [(3 PDAl₂)Ag][OTf] ([Ag][OTf]), suggesting that [BPh₄] extracted an equivalent of Ag⁺ to precipitate AgBPh₄ along with an equivalent of NaOTf. The metrics of [Ag][OTf] are listed in Table 3. The Ag atom lies in a planar geometry ($\Sigma \triangle N$ -Ag-N = 362.5°, Fig. 2a) and is

coordinated by the two N_{py} atoms (avg. $d(Ag-N_{py}) = 2.324 \text{ Å}$) and two neighboring N_{ald} atoms (avg. $d(Ag-N_{ald}) = 2.435 \text{ Å}$). Unlike the geometry of [(3PDAI₂)Sr][OTf]₂,^[12g] in which all six nitrogen atoms are coordinated to the metal center, the tetracoordination of the ³PDAl₂ ligand in [Ag][OTf] allows for more conformational flexibility in the aldimine groups and the propylene linker that contained the unbound nitrogens. This flexibility resulted in the lone pairs of the unbound Nald pointing away from the metal center to yield a conformation that allows N_{py} to more closely approach the metal center in the pocket of the macrocycle (2.32 Å vs 2.52 Å in $\{[Ag_2(NCMe)][OTf]_2\}_n$). The Δ_{expt} of the ligand is 0.174 Å, almost identical to that of $\{[Ag_2(NCMe)][OTf]_2\}_n$, and is indicative of a neutral ligand. NMR spectroscopic studies revealed that [Ag][OTf] also exhibits D_{2h}-symmetry in THF-d₈ and CD₃CN solutions at room temperature, as shown by the 8:4 pattern of the signals from the protons on the CH2CH2CH2 linkers (see Experimental Section and ESI Figures S7 and S12), but the data do not match those observed for $\{[Ag_2(NCMe)][OTf]_2\}_n$ under analogous conditions.

Scheme 4. Synthesis of mononuclear Ag complexes.

Interestingly, the addition of 2.1 equiv. of NaBPh4 to a stirring slurry of $\{[Ag_2(NCMe)][OTf]_2\}_n$ in THF did not remove the second Ag+ ion but instead resulted in the formation of a different monosilver complex, [(3PDAI₂)Ag(BPh₄)] ([Ag(BPh₄)]) (Scheme 4), in 56% yield. The molecular structure and crystallographic metrics of [Ag(BPh4)] are very similar to those of [Ag][OTf] (Fig. 2b, Table 3), but their ¹H NMR spectra in THF-*d*₈ exhibited modest, but non-negligible, shifts in the signals corresponding to the ³PDAl₂ ligand (Fig. S12 and S14, respectively); these changes would not be expected on exchange of two outer-sphere anions. Examination of the crystal structure of [Ag(BPh₄)] revealed a contact between the Ag center and one phenyl ring of the [BPh4] anion (Fig. 2b). The phenyl ring is η^2 -coordinated to the Ag(I) center through the C₄₃–C₄₂ bond (d(Ag···Ct_{C42C43}) = 2.818 Å, Ct =centroid). While this distance is on the longer end of Ag-based cation- π interactions, [19] the difference between the ¹H NMR data for the ³PDAI₂ signals in the two mononuclear compounds suggests that cation- π interactions may exist in solution for [Ag(BPh₄)]. Only one set of ¹H NMR spectroscopic signals were observed for the phenyl protons on the [BPh₄] anion at room temperature, which indicates the presence of a dynamic exchange process that may involve a change in the coordination mode of the phenyl rings to the Ag center in solution.

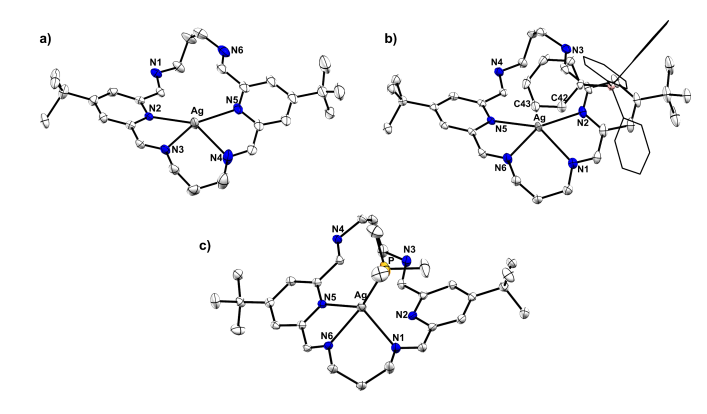


Figure 2. Crystal structures of a) the cationic portion of [Ag][OTf], b) [Ag(BPh₄)] and c) the cationic portion of [Ag(PMe₃)][OTf], with thermal ellipsoids at the 50% probability level. For clarity, the hydrogen atoms on all structures were omitted and three of the four aryl groups on the BPh₄ ion in (b) were depicted without thermal ellipsoids.

Table 3. Averaged crystallographic metrics of mononuclear Ag complexes.

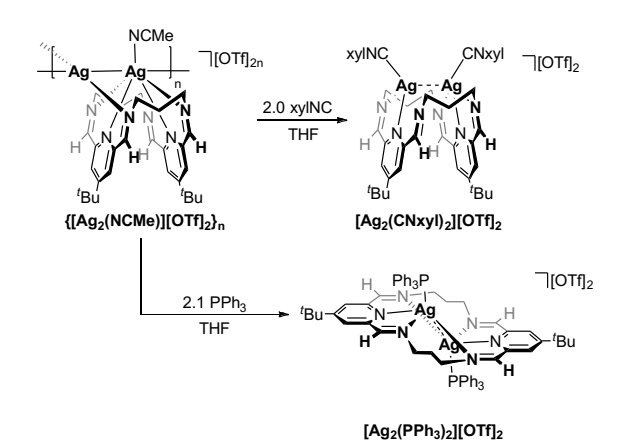
	[Ag][OTf]	[Ag(BPh ₄)]	[Ag(PMe ₃)][OTf]
d(Ag–L) ^a / Å	-	2.818	2.3614(6)
d(Ag-N _{py}) / Å	2.324	2.393	2.3839(14)
$d(Ag-N_{ald})$ / Å	2.435	2.402	2.397
d(N _{py} -C _{ipso}) / Å	1.345	1.346	1.346
$d(C_{ipso}\text{-}C_{ald})$ / Å	1.478	1.481	1.479
$d(C_{ald}\text{-}N_{ald})$ / Å	1.260	1.259	1.268
Δ _{expt} / Å	0.174	0.178	0.172

 $a L = Ct_{C42C43}$, P

Finally, loss of an equivalent of Ag from {[Ag2(NCMe)][OTf]2}n was also effected by addition of the Lewis base PMe₃. Treatment of {[Ag2(NCMe)][OTf]2}n with 2.4 equiv. of PMe3 in THF resulted in a pale golden yellow solution. Layering this solution with *n*-hexane at room temperature did not afford crystalline material. We reasoned that a dynamic processes in solution involving reversible PMe₃ binding^[12d] may be hampering crystallization. Repeating the crystallization in the presence of a slight excess of PMe₃ led to the formation of long, rod-like, colorless crystals. A crystallographic analysis revealed the formation of a phosphinecoordinated mono-silver complex, [(3PDAI2)Ag(PMe3)][OTf] ([Ag(PMe₃)][OTf]) (Fig. 2c). The silver center in this complex adopts a distorted tetrahedral geometry (τ_4 = 0.65) and is coordinated by PMe3, one N_{py} atom, and two N_{ald} atoms from adjacent positions on different PDAI moieties. The ³PDAI₂ ligand in this complex adopts a ligand conformation that is similar to that in [Ag][OTf], in which two of the aldimine nitrogen lone pairs are pointed away from the metal center. The Δ_{expt} value of 0.172 (Table 3) for the ligand in the PMe₃ adduct corresponds to a (³PDAl₂)⁰ physical oxidation state on the ligand.

Synthesis of Dinuclear Ag Complexes

The different ¹H NMR spectra of {[Ag₂(NCMe)][OTf]₂}_n and [Ag][OTf] in CD₃CN (Figures S1 and S7) indicated that {[Ag₂(NCMe)][OTf]₂}_n was not merely dissociating into [Ag][OTf] and solvated AgOTf in solution. This led us to investigate the possibility of using $\{[Ag_2(NCMe)][OTf]_2\}_n$ to access other dinuclear Ag complexes. Treatment of a slurry of $\{[Ag_2(NCMe)][OTf]_2\}_n$ in THF with ca. 2 equiv. of either PPh₃ or 2,6-dimethylphenyl isocyanide (xyINC) resulted in pale yellow solutions. Upon layering with *n*-hexane at room temperature, crystals of the dinuclear Ag complexes [(3PDAI₂)Ag₂(PPh₃)₂][OTf]₂ ([Ag₂(PPh₃)₂][OTf]₂)and [(3PDAl₂)Ag₂(CNxyl)₂][OTf]₂ ([Ag₂(CNxyI)₂][OTf]₂)were isolated (Scheme 5). crystallographically determined bond metrics of these two dinuclear species are summarized in Table 4. In the crystal structure of [Ag2(PPh3)2][OTf]2, the 3PDAI2 ligand adopts a stairlike conformation (Fig. 3a). Unlike previously reported stair-like complexes bound by this ligand class, [12e] in which each metal center is coordinated to three coplanar nitrogen atoms from one PDI moiety, each Ag center in [Ag2(PPh3)2][OTf]2 is coordinated to PPh3, two nitrogen atoms from one PDAI unit and an Nald atom from the other PDAI unit, creating a geometry that is best described as distorted tetrahedral (avg. τ_4 = 0.79) if the Ag···Ag interaction is neglected. If included, the geometry is distorted square pyramidal (avg. 75 = 0.07) with PPh₃ occupying the apical position. The Δ_{expt} value of $[Ag_2(PPh_3)_2][OTf]_2$ is 0.167 Å, indicating a very slight increase of electron density held on the formally (3PDAI₂)⁰ ligand. The Ag...Ag distance is 3.1516(2) Å, which is on the long end of the range of related distances in complexes with similar Ag coordination environments (pentacoordinate Ag in an N₃Ag coordination sphere) as revealed by a search in the CSD database (avg. d(Ag.Ag) = 3.012 Å, $\sigma = 0.164$ Å, N = 228).[19] This value is notably longer than that observed in {[Ag2(NCMe)][OTf]2}n and may be discussed in terms of the formal shortness ratio (FSR), defined as the distance between the two atoms divided by the sum of their single bond covalent radii. [20] The FSR value of the Ag...Ag contact in [Ag2(PPh3)2][OTf]2 is 1.18, indicative of a weak interaction between the Ag centers that could result from a d10-d10 metallophilic interaction, which is in good agreement with the Ag...Ag distance being smaller than twice the van der Waals radius of Ag (5.06 Å), as discussed above. [4, 17] The ¹H NMR spectrum of [Ag₂(PPh₃)₂][OTf]₂ in CD₃CN (Fig. S25) revealed that this complex exhibits averaged D_{2h} symmetry in solution, as shown by the broad singlets at 3.77 ppm (8H) and at 2.15 ppm (4H) arising from the proton signals of the propylene linker. The ³¹P{¹H} spectrum of [Ag₂(PPh₃)₂][OTf]₂ shows a very broad singlet signal at 9.73 ppm (Fig. S29). The higher symmetry in solution than in the solid state (C_i symmetry) and the broad signal in the complex's ³¹P{¹H} NMR spectrum are consistent with the presence of a fast dynamic exchange process that involves phosphine dissociation and/or migration.



Scheme 5. Synthesis of [Ag₂(PPh₃)₂][OTf]₂ and [Ag₂(CNxyI)₂][OTf]₂.

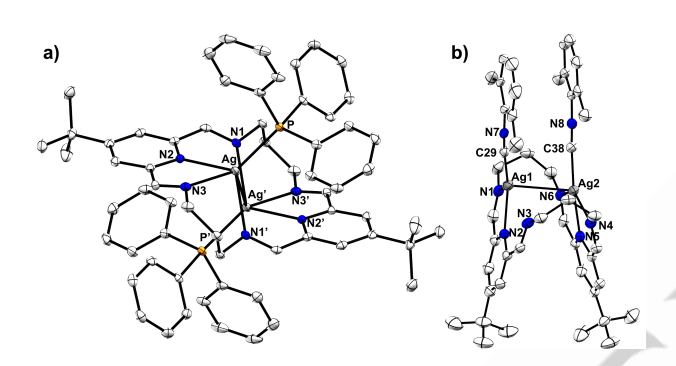


Figure 3. Crystal structure of a) $[Ag_2(PPh_3)_2]^{2+}$ and b) $[Ag_2(CNxyI)_2]^{2+}$ with thermal ellipsoids at the 50% probability level. Hydrogen atoms were omitted for clarity.

In contrast to the stair-like geometry of the ligand in $[Ag_2(PPh_3)_2][OTf]_2$, the ligand in $[Ag_2(CNxyI)_2][OTf]_2$ adopts a folded conformation in the solid-state, as determined by crystallographic analysis (Fig. 3b). Ag1 is three-coordinate, bound to one xyINC ligand and the N_{py} and one N_{ald} atoms from one PDAI unit, as indicated by the difference between d(Ag1-N1) of 2.334(3) Å and d(Ag1-N3) of 2.822(3) Å. The Ag2 center is more symmetrically coordinated by the other PDAI moiety and exhibits a distorted square planar geometry (τ_4 = 0.35,[21] $\Sigma \angle L$ -Ag-L = 359.8°, L = N, C) if the Ag...Ag interaction is neglected. Such square planar coordination geometry is uncommon for Ag centers. [15] The aryl groups on each xyINC ligand are nearly parallel to each other (∠Ar-Ar = 4.07°). This may result from a π - π stacking interaction between the isocyanide aryl rings $(d(Plane_{aryl} \cdots Plane_{aryl}) = 3.486 \text{ Å}).^{[22]}$ The Δ_{expt} value of [Ag2(CNxyl)2][OTf]2 is 0.178 Å, which leads to the assignment of a neutral ³PDAl₂ ligand. The Ag···Ag distance of 3.1050(4) Å is slightly shorter than that in [Ag2(PPh3)2][OTf]2 but within the range reported in other disilver bis-isocyanide complexes, [23] and, as mentioned above, the corresponding FSR of 1.16 is consistent with a weak Ag-Ag interaction that can be classified as a metallophilic interaction.

[Ag₂(CNxyI)₂][OTf]₂ is *pseudo-C*_{2v}-symmetric in the solid state, but its ¹H NMR spectrum in CD₃CN at room temperature exhibits higher symmetry, as shown by both a broad singlet at 4.06 ppm (8H), attributable to the signals from the H atoms on the

(CH₂)₃ linkers that are α to the aldimine nitrogen atoms, and a very broad and low-intensity signal at 2.68 ppm (4H), assignable to the central H atoms on the linker (Fig. S31). This increase in symmetry over that observed in the solid-state again suggests that a dynamic process is occurring in solution at room temperature, prompting an investigation into the mechanism of this process.

 $\label{table 4. Crystallographic metrics for $[Ag_2(PPh_3)_2][OTf]_2$ and $[Ag_2(CNxyI)_2][OTf]_2$.}$

	$[Ag_2(PPh_3)_2][OTf]_2$	[Ag ₂ (CNxyl) ₂][OTf] ₂
d(Ag···Ag) / Å	3.1516(2)	3.1050(4)
		2.078(4)
d(Ag–L) ^a / Å	2.4090(4)	2.086(4)
		2.304(3)
d(Ag-N _{py}) / Å	2.4039(12)	2.285(3)
	2.4328(12)	2.334(3)
d(Ag-N _{ald}) / Å	2.4326(12)	2.484(3)
J(Ay-Nald) / A	2.3986(13)	2.582(3)
		1.345(5)
	1.3479(19)	1.335(5)
d(N _{py} -C _{ipso}) / Å	1.3476(19)	1.334(50
		1.333(5)
		1.476(6)
	1.477(2)	1.476(6)
d(C _{ipso} -C _{ald}) / Å	1.475(2)	1.472(6)
		1.480(6)
		1.256(5)
	1.2731(19)	1.257(5)
$d(C_{\text{ald}}\text{-}N_{\text{ald}})$ / Å	1.269(2)	1.271(5)
	255(2)	1.255(5)
Δ _{expt} / Å	0.167	0.178
FSR	1.18	1.16
<i>T</i> 4	0.79	0.35 ^b

 $[^]a$ L = P for $[Ag_2(PPh_3)_2][OTf]_2$ and C for $[Ag_2(CNxyI)_2][OTf]_2.$

Solution-Phase Dynamics of [Ag₂(CNxyI)₂][OTf]₂

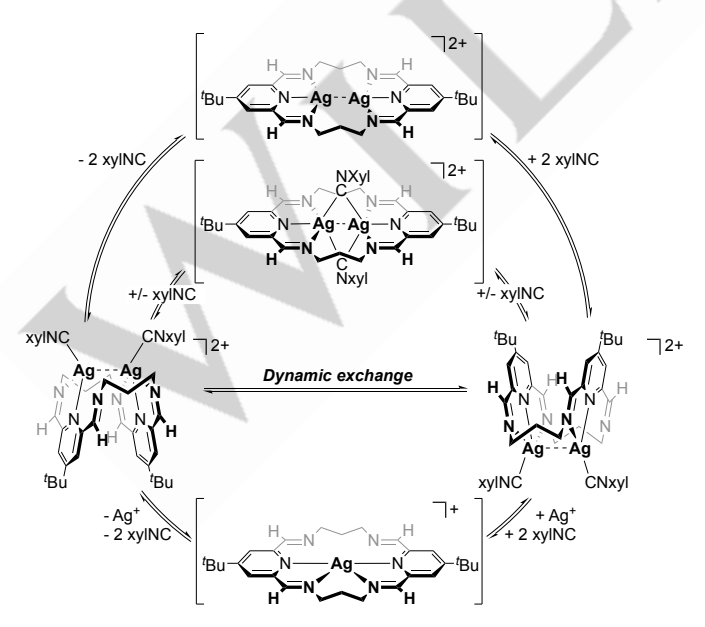
The higher symmetries observed for [Ag₂(PPh₃)₂][OTf]₂ and [Ag₂(CNxyI)₂][OTf]₂ on the NMR timescale in solution compared to their solid-state structures, along with the broadened NMR spectral resonances for these complexes in solution at room temperature, indicated the presence of a solution-phase dynamic exchange process that allows for changes in PDAI fragment denticity, 3 PDAI₂ ligand conformation, and Lewis base binding to the [Ag₂(L)₂]²⁺ core (L = PPh₃, xyINC). It was unclear, however, if these exchange processes involve ligand dissociation, Ag⁺ ion dissociation, or both, prompting us to study the mechanism of

^b Data for Ag2.

dynamic exchange at one of these species, the isocyanide complex [Ag₂(CNxyI)₂][OTf]₂.

The averaged D_{2h} symmetry observed in solution for [Ag2(CNxyI)2][OTf]2 indicates that the dynamic exchange process occurring in solution must involve a change in ligand conformation that allows for equilibration of the linker protons, which are diastereotopic in the solid-state. This must then involve the dissociation/re-association of some portion of the $[Ag_2(CNxyI)_2]^{2+}$ core. Based on this analysis, we propose two mechanistic classes. In the first, the dinuclear core remains intact, forming either the base-free complex [Ag2]2+ or a trans form of [Ag2(CNxyI)2]2+ in which one isocyanide has dissociated and reassociated with the opposite face of the complex. These species would then undergo a ³PDAl₂ ligand conformation change before both xyINC ligands rebind to the dinuclear core in a cis fashion. In the second mechanistic class, the loss of one Ag⁺ ion generates a mononuclear complex, $[Ag(CNxyI)_x]^+$ (x = 0, 2). Subsequent inversion of the ³PDAl₂ ligand, followed by reassociation of the free Ag+ ion (and isocyanide ligands) would then reform [Ag2(CNxyI)2]2+ (Scheme 6). The isolation of the monosilver complex [Ag][OTf] allowed us to differentiate between these two mechanistic classes.

The interaction between [Ag][OTf] and xyINC was studied first. Sequential addition of up to 2.62 equiv. of xyINC to a THF- d_8 solution of [Ag][OTf] revealed both a shift in all diamagnetic peaks and only one set of signals attributable to xyINC, consistent with a fast equilibrium involving [Ag][OTf], xyINC and [Ag(CNxyI)x][OTf] (Fig. S13). Treatment of a THF- d_8 solution of [Ag][OTf] with 2.0 equiv. of xyINC, followed by the subsequent addition of 1.0 equiv. of AgOTf, however, did not afford [Ag2(CNxyI)2][OTf]2 (Fig. 4), indicating that the binding of Ag⁺ and xyINC to the mononuclear species [Ag(CNxyI)x][OTf] to form [Ag2(CNxyI)2][OTf]2 is not feasible at room temperature. As such, we favor a ligand dissociation and re-association process in which the complex maintains a dinuclear core, *i.e.* the dinuclear mechanism, as the dominant class of dynamic exchange between conformers of [(Ag2(CNxyI)2)[OTf]2 in solution.



Scheme 6. Examples of possible mechanisms of the dynamic exchange behavior of [Ag₂(CNxyI)₂][OTf]₂ in solution.

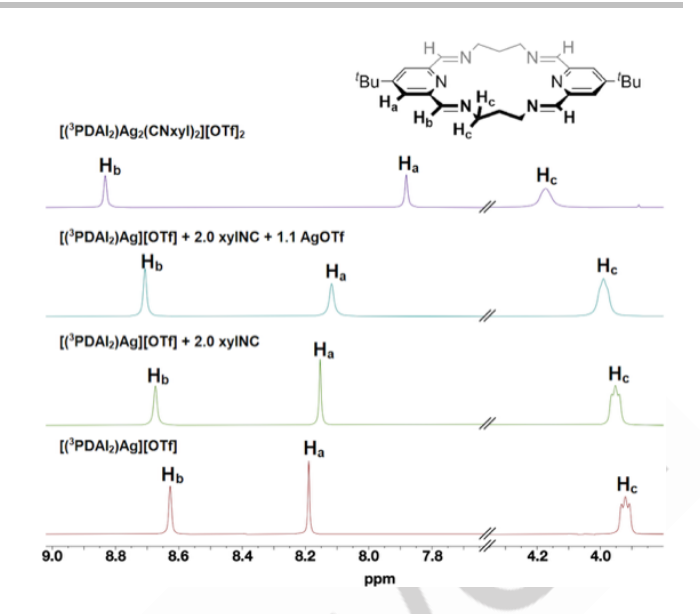


Figure 4. Abbreviated 1H NMR spectra resulting from the sequential addition of xyINC and AgOTf into a THF- d_8 solution of [Ag][OTf] at room temperature. The 1H NMR spectra of [Ag][OTf] and [Ag2(CNxyI)2][OTf]2 in THF- d_8 at room temperature are provided for comparison. 1H signals from corresponding hydrogen atoms on the 3PDAI_2 ligand and labeled for clarity. For full spectra see Fig. S36.

Computational Analysis

To further probe the interaction between the Ag centers in $[Ag_2(L)_2][OTf]_2$ (L = PPh₃, xylNC), various levels of theory were used to analyze $[Ag_2(CNxyI)_2][OTf]_2$ and $[Ag_2(PPh_3)_2][OTf]_2$. Single point energy calculations were carried out on the coordinates generated from the crystal structures at the B97-D3/ZORA-def2-TZVP level of the theory. The ZORA-def2-TZVP basis set was applied to include relativistic effects, and the D3 dispersion correction was used to include the effects of dispersion, which is an important factor to be considered when investigating metallophilic interactions. [5c, 24]

Careful examination of the frontier orbitals of the disilver complexes revealed important differences from previously reported diiron, dicobalt and dinickel complexes. The ligand π^* orbitals are extensively mixed with the metal d-manifold in the iron, cobalt and nickel complexes,[12d] which results in significant electron density delocalization onto the ³PDI₂ ligand. However, in the case of the disilver complexes, only minimal ligand π^* orbital mixing with the silver d-manifold was observed. No ³PDAI₂ ligand π^* orbital mixing was found from HOMO to HOMO-20 for $[Ag_2(PPh_3)_2][OTf]_2$ or $[Ag_2(CNxyI)_2][OTf]_2$. This is further supported by the Mulliken population analyses on these complexes, which gave overall charges of +0.89 and +1.06 on the Ag₂ moiety, and +0.64 and +0.54 on the ³PDAl₂ ligands in [Ag2(PPh3)2][OTf]2 and [Ag2(CNxyI)2][OTf]2, respectively. In fact, the LUMO to LUMO+3 of both disilver complexes show predominantly ligand π^* character (Fig. S43 and S45), while the HOMO orbitals show the σ -symmetry interactions between ligand-based fragments and the Ag d-manifolds (Fig. S44 and S46). As a result, the redox-active PDAI moieties on the ligand are not predicted to influence the Ag...Ag interaction in the bimetallic core, due to the minimal mixing of ligand π^* character with Ag₂-based orbitals.

Further, DFT predicts no net covalent bonding between the metal centers in either complex, leaving the possibility of a non-covalent, argentophilic interaction between the two d¹0 ions. The macrocyclic ligand system supporting the disilver complexes complicates an energy decomposition analysis of the Ag···Ag interaction, which usually requires two Ag atoms to be in independent fragments. We thus turned to the Quantum Theory of Atoms in Molecules (QTAIM), l²6| which was used as an alternative way to obtain insight into the Ag···Ag interactions.

The QTAIM analyses of both [Ag2(CNxyI)2][OTf]2 and [Ag2(PPh3)2][OTf]2 revealed bond critical points (BCPs) between each pair of silver centers. The properties of the BCPs are listed in Table 5. This table lists values for ρ_b and $\nabla^2 \rho$, the electron density and the Laplacian of the electron density at the BCP, respectively, as well as G_b , V_b , and H_b , which represent the kinetic energy density, potential energy density and energy density at the BCP. These five parameters, when used together, can be used to define the nature of the interaction between two atoms. For example, relatively large-positive ρ_b values and large-negative $\nabla^2 \rho_b$ values are typical of covalent bonds. The C–C single bond between the two ethyl groups in *n*-butane, for example, is characterized by a ρ_b of 0.241 e•Å⁻³ and $\nabla^2 \rho_b$ of -0.510 e•Å⁻⁵.[27] In contrast, the interactions between the silver centers in the present dinuclear Ag complexes are characterized by ρ_b values that are nearly an order of magnitude smaller. Additionally, the positive $\nabla^2 \rho_b$ values suggest the presence of non-covalent, closed-shell interactions. [28] Butcher and co-workers reported QTAIM analysis results on a series of complexes featuring d10...d10, d10...d8 and $d^8 \cdots d^8$ metallophilic interactions. [6a] The ρ_b values of these interactions are within the range of 0.033 to 0.055 e-A-3, and the $\nabla^2 \rho_b$ values are all positive, ranging from 0.066 to 0.146 e•Å⁻³. These closed-shell interactions can be further classified by the values of G_b , V_b and H_b at the BCP, according to the classification of atomic interactions developed by Marabello and coworkers. [28] The corresponding values for the BCP of the Ag...Ag interactions in $[Ag_2(CNxyI)_2][OTf]_2$ and $[Ag_2(PPh_3)_2][OTf]_2$ (Table 5) are in line with those reported for other d10-d10 metallophilic interactions. [6a] Therefore, the Ag...Ag interactions in the dinuclear Ag complexes are best described as metallophilic in both cases.[8a][29]

Table 5. Properties of the bond critical points between Ag centers in $[Ag_2(CNxyI)_2][OTf]_2$ and $[Ag_2(PPh_3)_2][OTf]_2$.

	$[Ag_2(PPh_3)_2][OTf]_2$	[Ag ₂ (CNxyI) ₂][OTf] ₂
ρ _b /e•Å-³	0.014	0.016
$ abla^2 ho_{ m b}/{ m e}$ •Å-5	0.035	0.040
G _b /hartree•Å⁻³	0.010	0.011
V _b /hartree•Å⁻³	-0.011	-0.012
H₀ /hartree•Å-³	-0.001	-0.001

Bond order analyses were next used to gain further insight into the strength of the metallophilic interactions in the disilver complexes and investigate how the difference in the metallophilic interactions might affect the conformation of the ligand. The Mayer Bond Order (MBO) of the Ag···Ag interaction in

 $[Ag_2(PPh_3)_2][OTf]_2$ was calculated to be 0.1247, smaller than that in $[Ag_2(CNxyI)_2][OTf]_2$ (0.1722), indicating a weaker metallophilic interaction in the former complex (Table 6).

Table 6. Calculated bond order indices of the Ag···Ag interactions in $[Ag_2(CNxyI)_2][OTf]_2$ and $[Ag_2(PPh_3)_2][OTf]_2$.

	[Ag ₂ (PPh ₃) ₂][OTf] ₂	[Ag ₂ (CNxyl) ₂][OTf] ₂
Mayer Bond Order	0.1247	0.1722
Intrinsic bond strength index	0.0217	0.0218

The Independent Gradient Model-based Hirshfeld partition (IGMH) method^[30] was used to visualize the weak interaction between the Ag centers as a way of corroborating the QTAIM and bond-order analyses. The weak interaction between the metal centers was analyzed by dividing the disilver core in the two complexes into two fragments, each containing one Ag center and the L-type ligand (PPh3, CNxyl) coordinated to the Ag center. IGMH isosurfaces showing the inter-fragment interactions were then obtained. For both complexes, the IGMH isosurface at an isovalue of 0.01 reveals density between the Ag centers (Fig. 5), indicating that the Ag...Ag interaction is the predominant contributor to the attractive inter-fragment interactions. The $sign(\lambda_2)\rho$ values for each isosurface (Fig. 5, green color) indicate, however, that the electron density at each is nearly zero, further supporting the non-covalent nature of the interaction between Ag centers in these complexes.

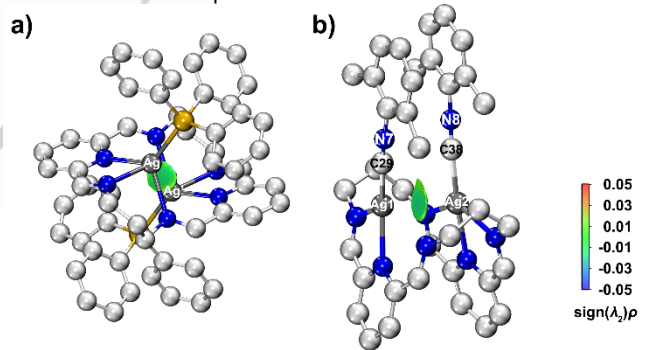


Figure 5. IGMH isosurfaces between two AgL fragments of a). **[Ag₂(PPh₃)₂][OTf]₂** and b). **[Ag₂(CNxyI)₂][OTf]₂**. The isosurfaces are plotted at an isovalue of 0.01 and colored with respect to the corresponding $sign(\lambda_2)\rho$ values. The color bar is shown at the right of the figure.

To further evaluate and compare the strength of the weak Ag···Ag interactions, the intrinsic bond strength index (IBSI)^[31] was calculated. The IBSI value of the Ag···Ag interaction of [Ag₂(PPh₃)₂][OTf]₂ is calculated to be 0.0217, while that of [Ag₂(CNxyI)₂][OTf]₂ is calculated to be 0.0218 (Table 6) and the Ag···Ag interaction of {[Ag₂(NCMe)][OTf]₂}n bears an IBSI value of 0.0318 (Table S4). All are an order of magnitude smaller than the IBSI values of the Ag–P and Ag1–C29 bonds in these complexes (0.1454 and 0.1936, respectively), consistent with their weak natures. The interaction energies of Ag···Ag metallophilic interactions have been widely studied computationally within N-heterocyclic carbene-coordinated ^[32] and phosphine-coordinated silver halide dimers^[11b, 11c, 33] in different

conformations. The energy of the Ag...Ag metallophilic interaction has been calculated to be ca. 15 kcal/mol at an optimized Ag···Ag distance of ca. 3.2 Å for the staggered [(H₃P)AgCl]₂ dimer.^[11b] Similarly, in the [(NHC')AgCl]₂ dimer (NHC' = 1,3,4-trimethyl-4,5dihydro-1H-1,2,4-triazol-5-ylidene), an interaction energy of 22.6 kcal/mol at a Ag...Ag distance of 3.16 Å was calculated, but an estimation of the energy of the Ag...Ag interaction was complicated by the extra interactions between Ag and NHC' moieties.[32] It would be beneficial to place the IBSI values of the Ag...Ag interactions in [Ag₂(PPh₃)₂][OTf]₂[Ag2(CNxyI)2][OTf]2 in context with respect to those reported in the literature. Therefore, we examined the IBSI value of the Ag···Ag interaction of [(NHC)AgCl]₂ (NHC = 1-(benzyl)-3(N-tertbutylacetamido)imidazole-2-ylidene), reported by Ghosh and coworkers. [11a] This complex adopts a head-to-tail conformation with a d(Ag···Ag) of 3.1970(12) Å. The Ag···Ag interaction energy for this species was estimated to be 12.8 kcal/mol, and its IBSI value was calculated to be 0.0184 (Table S4), which is slightly smaller than those calculated for [Ag2(PPh3)2][OTf]2 and [Ag2(CNxyI)2][OTf]2. Therefore, a lower limit of the energy of the Ag...Ag interaction in these complexes could be estimated to be ca. 12.8 kcal/mol. The minimal difference between the two Ag...Ag IBSI values in the ³PDAI₂-ligated complexes indicates that the strengths of the Ag...Ag interactions of [Ag2(PPh3)2][OTf]2 and [Ag2(CNxyI)2][OTf]2 are almost identical, which, however, does not explain the difference in the conformation of the macrocyclic ligand between $[Ag_2(PPh_3)_2][OTf]_2$ and $[Ag_2(CNxyI)_2][OTf]_2$.

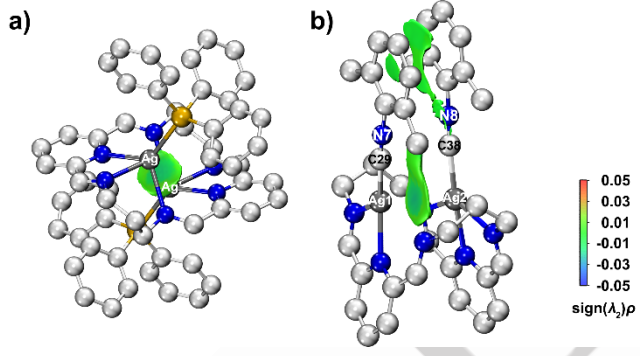


Figure 6. IGMH isosurfaces (plotted at an isovalue of 0.005 and colored with respect to the corresponding $sign(\lambda_2)\rho$ value) between two AgL fragments of a). [Ag₂(PPh₃)₂][OTf]₂ and b). [Ag₂(CNxyI)₂][OTf]₂. The color bar is shown at the right of the figure.

Further investigation using the IGMH method, but with the more inclusive isosurface value of 0.005, revealed secondary and non-negligible π -stacking interactions between the L-type xyINC ligands in [Ag₂(CNxyI)₂][OTf]₂ that are absent [Ag2(PPh3)2][OTf]2 (Fig. 6). In the scope of the IBSI analysis, there is difficulty describing the strength of this interaction.[31] However, the C29···C38 interaction is calculated to be the predominant contributor to this secondary interaction with an IBSI value of 0.005. Though smaller than the IBSI values for the Ag...Ag interactions, the C29...C38 interaction should not be neglected, as this value is ~25% of that of the IBSI value of the metallophilic interactions themselves and the entire π -stacking interaction between the xyINC ligands will be stronger than the lone C29...C38 interaction. It could thus be reasoned that the conformational difference between the two disilver complexes in the solid state is a result of this secondary, ligand...ligand interaction. Notably, however, this inter-ligand interaction is weak and would not prevent the dynamic ligand conformational exchange observed in solution.

Conclusion

Silver complexes with various solid-state conformations (folded and unfolded) and nuclearities (mononuclear, dinuclear and linear polymeric) supported by the ³PDAl₂ macrocyclic ligand were successfully synthesized and characterized. The chain-containing species {[Ag₂(NCMe)][OTf]₂}_n was found to exist in a monomeric form in solution and proved to be an effective precursor for the syntheses of variable-nuclearity molecular complexes. Of these, the disilver complexes, which benefitted from the robust macrocyclic ligand framework, were found to exhibit dynamic exchange processes in solution involving ligand conformational changes as well as dissociation and reassociation of monodentate L-type donors. The dynamic solution-phase behaviors of these disilver complexes were studied by various NMR spectroscopy techniques and found to retain their disilver formulation in solution, despite the possibility of Ag⁺ loss during isomerization.

The electronic structures of the disilver complexes were investigated computationally. Minimal mixing of ³PDAl₂ ligand π* character into the occupied molecular orbitals results in neutral ³PDAl₂ ligands in the Ag complexes as opposed to previously reported Fe, Co and Ni complexes.[12a-f] The Ag...Ag interactions in the disilver complexes were shown to be non-covalent, and QTAIM analyses suggested the presence of metallophilic interactions between the Ag centers. These interactions were further probed by IGMH and IBSI analyses, which revealed attractive interactions between the two Ag-L fragments in the disilver complexes featuring predominantly Ag···Ag interactions with almost identical strength. The inter-ligand interaction present in [Ag2(CNxyl)2][OTf]2 but absent in [Ag2(PPh3)2][OTf]2 is reasoned to be the main contributor to the conformation difference between the two complexes. This result complements our past observations that the energy difference associated with ligand folding and unfolding in this class of complexes is minimal, indicating that this ligand system may be used to signal both the strength of metal-metal interactions but also the strength of interligand interactions.

Experimental Section

General Methods. All reactions were performed under an inert atmosphere of dry N2 in an Inert PureLab HE glovebox or using standard Schlenk techniques unless otherwise noted. Glassware, stir bars, filter aid (Celite) and 4 Å molecular sieves were dried in an oven at 150 °C for at least 12 h prior to use. All solvents (n-hexane, diethyl ether, THF, dichloromethane, acetonitrile) were dried by passage through a column of activated alumina, deoxygenated by sparging with N2 for 15 min, and stored over 4 Å molecular sieves unless otherwise noted. Deuterated solvents were purchased from Cambridge Isotope Laboratories, Inc., and either i) dried over either Na/benzophenone (THF-d₈) or CaH₂ (acetonitrile-d₃) and stored under N₂ over activated 4 Å molecular sieves or ii) used as received (methanol-d₄). synthesized following published [(³PDAl₂)Sr][OTf]₂ was procedures.[12g] AgNO₃ (99.9%-Ag), and NaBPh₄ (99.5%+) were

purchased from Strem Chemicals and used without further purification. 2,6-dimethylphenyl isocyanide (xyINC) purchased from Alfa Aesar and used without further purification. PMe₃, which was either purchased from Strem Chemicals (98%) or synthesized according to a literature procedure, [34] was stored as a 1 M solution in THF at -35 °C under dry nitrogen in a glovebox. PPh₃ was purchased from MilliporeSigma, recrystallized from hot ethanol, dried at 40 °C under vacuum (30 mbar) for 6h, and stored in a glovebox under dry nitrogen prior to use.[35] 1,3,5trimethoxybenzene was purchased from Alfa Aesar, recrystallized twice from n-hexane, dried at 60 °C under vacuum (30 mbar) for 10 h and stored in a glovebox under dry nitrogen prior to use. [35] Elemental analyses were performed under an inert atmosphere by Midwest Microlab, LLC or at the University of Rochester (PerkinElmer 2400 Series II). ¹H, ¹³C{¹H}, ¹¹B{¹H}, ³¹P{¹H}, ¹⁹F{¹H}, ¹H DOSY, ¹³C-¹H HSQC, ¹³C-¹H HMBC and ¹H-¹H COSY NMR spectra were recorded on Bruker UNI 400, UNI 500 or NEO 600 spectrometers. All chemical shifts (δ) are reported in units of ppm. with references to the residual protio-solvent resonance for proton and carbon chemical shifts. External BF3•Et2O. H3PO4 and CFCl3 were used for referencing ³¹P and ¹⁹F NMR chemical shifts, respectively.

All density functional theory (DFT) calculations were performed with the ORCA program package, v3.0.3.[36] Single point energy calculations were carried out at the B97-D3 level of theory,[37] using model compounds derived from crystallographic data. All tert-butyl groups were truncated to a hydrogen atom to minimize computational expense. The ZORA-def2-TZVP basis set was used for Ag, and the def2-TZVP basis sets were used for the atoms connected to Ag. [38] All other atoms were described using the def2-SV(P) basis sets. The Conductor-like Screening Model (COSMO; dipole moment corresponding to acetonitrile) was implemented throughout. The SCF calculations were tightly converged (1x10⁻⁸ Eh in energy, 1x10⁻⁷ Eh in the density change, and 5x10⁻⁷ in the maximum element of the DIIS error vector). Orbital plots were generated using the program Chimera, [39] with isosurface cutoffs of |0.03| a.u. QTAIM, Mayer Bond Order, IGMH, IBSI and Mulliken population analyses were carried out with the Multiwfn 3.8 package (dev release, 2022/04/06).[40] IGMH isosurface plots were generated using VMD 1.9.3.[41]

X-ray Crystallography. X-ray intensity data were collected on a Bruker D8QUEST CMOS ($\{[Ag_2(NCMe)][OTf]_2\}_n$) or a XtaLAB ([Ag][OTf], Rigaku Synergy-S [Ag(BPh₄)], [Ag(PMe₃)][OTf], [Ag₂(PPh₃)₂][OTf]₂ and [Ag₂(CNxyI)₂][OTf]₂) diffractometer equipped with an HPC area detector (Dectris 200K), with graphite-monochromated R $(\{[Ag_2(NCMe)][OTf]_2\}_n)$ confocal multilayer opticor monochromated ([Ag][OTf], [Ag(BPh4)], [Ag(PMe3)][OTf], [Ag₂(PPh₃)₂][OTf]₂ and [Ag₂(CNxyI)₂][OTf]₂) Mo Kα radiation $(\lambda = 0.71073 \text{ Å})$ at 100 K. Rotation frames were integrated using SAINT^[42] ($\{[Ag_2(NCMe)][OTf]_2\}_n$) or CrysAlisPro^[43] ($[Ag][OTf]_n$, [Ag(PMe₃)][OTf], [Ag₂(PPh₃)₂][OTf]₂[Ag(BPh₄)], [Ag2(CNxyI)2][OTf]2), producing a listing of unaveraged F2 and $\sigma(F^2)$ values. The intensity data were corrected for Lorentz and polarization effects and for absorption using SADABS[44] $(\{[Ag_2(NCMe)][OTf]_2\}_n)$ or SCALE3 ABSPACK^[45] ([Ag][OTf],[Ag₂(PPh₃)₂][OTf]₂ [Ag(PMe₃)][OTf], [Aa(BPh4)]. [Ag2(CNxyI)2][OTf]2). The structures were solved by direct methods by using SHELXT^[46] and refined by full-matrix least F^2 SHELXL-2014^[46] based on using SHELXL-2018^[46] $(\{[Ag_2(NCMe)][OTf]_2\}_n)$ or ([Ag][OTf], [Ag(BPh4)], [Ag(PMe3)][OTf], [Ag2(PPh3)2][OTf]2 and [Ag2(CNxyI)2][OTf]2). Crystal parameters and refinement results are given in Tables S1-S3.

 ${[(^3PDAI_2)Ag(NCMe)Ag][OTf]}_n$ **Synthesis** $(\{[Ag_2(NCMe)][OTf]_2\}_n)$. AgNO₃ (87.6 mg, 0.544 mmol) and [(3PDAI₂)Sr][OTf]₂ (203.3 mg, 0.241 mmol) were mixed in 6 mL of MeCN under air in a 20 mL scintillation vial equipped with a stir bar. The vial was wrapped with aluminum foil after mixing the reagents, and the reaction mixture was stirred in the dark at room temperature for 2 h. The resulting yellow slurry was filtered through Celite. The filtrate was layered with 12 mL of anhydrous diethyl ether. Storage of the system at room temperature for 2 days in the dark yielded $\{[Ag_2(NCMe)][OTf]_2\}_n$ as an off-white powder. Yield: 121.4 mg (50%). 1H NMR (500 MHz, CD₃CN, 25 °C): δ = 8.38 (s, 4H, CH=N), 7.76 (s, 4H, py m-H), 3.94 (t, ${}^{3}J_{HH}$ = 4.5 Hz, 8H, $CH_2CH_2CH_2$), 2.41 (quint, $^3J_{HH}$ = 5.2 Hz, 4H, $CH_2CH_2CH_2$), 1.31 (s, 18H, $C(CH_3)_3$) ppm. ¹³ $C\{^1H\}$ NMR (126) MHz, CD₃CN, 25 °C): δ = 165.94 (s, py C), 161.48 (s, CH=N), 150.99 (s, py C), 125.54 (s, py m-C), 122.11 (q, ${}^{1}J_{FC}$ = 320.0 Hz, CF₃SO₃), 60.82 (s, CH₂CH₂CH₂), 36.09 (s, C(CH₃)₃), 30.39 (s, C(CH₃)₃), 30.07 (s, CH₂CH₂CH₂) ppm. Anal. Calcd. for $C_{32}H_{41}Ag_2F_6N_7O_6S_2 \ (1013.58 \ g/mol): \ C, \ 37.92; \ H, \ 4.08; \ N, \ 9.67.$ Found: C, 37.85; H, 3.89; N, 9.65. [(3PDAI2)Ag2(NCMe)][OTf]2 was dried at 40 °C under vacuum (30 mbar) for 6h and stored in a glovebox under dry nitrogen.

Synthesis of [(³PDAI₂)Ag][OTf] ([Ag][OTf]). {[Ag2(NCMe)][OTf]2}n (49.2 mg, 0.049 mmol) was dispersed in 6 mL of THF and stirred for 5 min before NaBPh4 (17.5 mg, 0.051 mmol) was added. The resulting white slurry was stirred for 2 h. The reaction mixture was then filtered through Celite. The filtrate was layered with 12 mL of n-hexane. Storage of the system at room temperature for 13 d afforded [Ag][OTf]-0.5 THF as golden needles. Yield: 19.0 mg (52%). ¹H NMR (600 MHz, CD₃CN, 25 °C): δ = 8.48 (s, 4H, CH=N), 8.05 (s, 4H, py m-H), 3.89 (t, ${}^{3}J_{HH}$ = 4.8 Hz, 8H, $CH_2CH_2CH_2$), 2.21 (quint, $^3J_{HH}$ = 4.6 Hz, 4H, $CH_2CH_2CH_2$), 1.41 (s, 18H, $C(CH_3)_3$) ppm. ¹³ $C\{^1H\}$ NMR (151) MHz, CD₃CN, 25 °C) δ = 165.64 (s, py C), 162.58 (s, CH=N), 152.85 (s, py C), 124.78 (s, py m-C), 122.18 (q, $^{1}J_{FC}$ = 321.6 Hz, CF₃SO₃), 60.13 (s, CH₂CH₂CH₂), 36.23 (s, C(CH₃)₃), 30.46 (s, $C(CH_3)_3)$, 30.43 (s, $CH_2CH_2CH_2$) ppm. ¹⁹ $F\{^1H\}$ NMR (376 MHz, CD₃CN, 25 °C): δ = -79.34 (s, CF₃SO₃) ppm. Anal. Calcd. for $C_{31}H_{42}AgF_3N_6O_{3.5}S$ (751.64 g/mol): C, 49.54; H, 5.63; N, 11.18. Found: C, 46.43; H, 5.06; N, 10.33. The unsatisfactory EA data may result from the presence of Ag salt byproducts (e.g. AgBPh₄), which show modest solubility in THF.

[(3PDAI₂)Ag(BPh₄)] **Synthesis** of $([Ag(BPh_4)]).$ ${[Ag_2(NCMe)][OTf]_2}_n$ (115.1 mg, 0.114 mmol) was dissolved in $6\;mL$ of MeCN and stirred for 5 min before NaBPh4 (81.0 mg, 0.237 mmol) was added. The resulting white slurry was stirred for 1 h. All volatile materials were removed under reduced pressure. Soluble materials were extracted from the solid residue with 6 mL of THF. The mixture was filtered through Celite, and the filtrate was layered with 12 mL of n-hexane. Storage of the system at room temperature for 4 days yielded [Ag(BPh4)] as golden needles. Yield: 56.0 mg (56%). ¹H NMR (600 MHz, THF-d₈, 25 °C): δ = 8.28 (s, 4H, C*H*=N), 8.04 (s, 4H, py *m*-H), 7.27 (m, 8H, Ph m-H), 6.81 (t, 8H, $^{3}J_{HH}$ = 7.4 Hz, Ph o-H), 6.65 (tt, 4H, $^{3}J_{HH}$ = 7.2 Hz, ${}^{5}J_{HH}$ = 1.6 Hz, Ph p-H), 3.78 (t, ${}^{3}J_{HH}$ = 4.8 Hz, 8H, $CH_2CH_2CH_2$), 2.14 (quint, $^3J_{HH} = 5.2 \text{ Hz}$, 4H, $CH_2CH_2CH_2$), 1.41 (s, 18H, C(CH₃)₃) ppm. ¹³C{¹H} NMR (151 MHz, THF-d₈, 25 °C): δ = 165.66 (s, py C), 165.45 (q, ${}^{1}J_{BC}$ = 49.3 Hz, BPh₄ C) 162.68 (s, CH=N), 153.06 (s, py C), 137.36 (m, BPh₄ *m*-C), 125.92 (q, ${}^{3}J_{BC}$ = 2.9 Hz, BPh₄ o-C), 124.89 (s, py m-C), 121.97 (s, BPh₄ p-C), 60.19 (s, CH₂CH₂CH₂), 36.40 (s, C(CH₃)₃), 30.74 (t, J = 10.4 Hz, CH₂CH₂CH₂) , 30.68 (s, C(CH₃)₃). ${}^{11}B_{1}^{4}H_{1}^{4}$ NMR (128 MHz, THF- d_{8} , 25 °C): δ = -8.90 (s, *B*Ph₄) ppm. Anal. Calcd. for C₅₂H₅₈AgBN₆ (885.76 g/mol): C, 70.51; H, 6.60; N, 9.49. Found: C, 70.46; H, 6.77; N, 9.59.

Synthesis of [(3PDAI₂)Ag(PMe₃)][OTf] ([Ag(PMe₃)][OTf]). $\{[Ag_2(NCMe)][OTf]_2\}_n$ (50.7 mg, 0.050 mmol) was dispersed in 6 mL of THF and stirred for 5 min before PMe₃ (1M in THF, 0.12 mL, 0.12 mmol) was added. The reaction mixture gradually turned into a golden yellow solution as it was stirred at room temperature for 1.5 h. All volatile materials were then removed under reduced pressure, and the soluble materials were extracted from the solid residue with 6 mL of THF. The mixture was filtered through Celite. An aliquot of a PMe3 solution (0.05 mL, 1 M in THF) was added to the filtrate, and the resulting pale goldenyellow solution was layered with 12 mL of n-hexane. Storage of the system at room temperature for 6 days yielded [Aq(PMe₃)][OTf]·THF as colorless needles. Yield: 25.6 mg (59%). ¹H NMR (500 MHz, CD₃CN, 25 °C): δ = 8.40 (s, 4H, CH=N), 7.98 (s, 4H, py m-H), 3.89 (t, ${}^{3}J_{HH}$ = 5.5 Hz, 8H, $CH_{2}CH_{2}CH_{2}$), 2.25 (br s, 4H, CH₂CH₂CH₂), 1.37 (s, 18H, C(CH₃)₃), 1.04 (br s, 9H, $P(CH_3)_3)$ ppm. ¹³C{¹H} NMR (126 MHz, CD₃CN, 25 °C): δ = 164.54 (s, py C), 163.20 (s, CH=N), 153.60 (s, py C), 124.03 (s, py m-C), 61.00 (s, $CH_2CH_2CH_2$), 36.00 (s, $C(CH_3)_3$), 30.48 (s, $C(CH_3)_3$), 30.28 (s, $CH_2CH_2CH_2$), 15.47 (d, $^1J_{PC}$ = 18.2 Hz, P(CH₃)₃). ³¹P{¹H} NMR (162 MHz, CD₃CN, 25 °C): δ = -40.70 (s, P(CH₃)₃) ppm. Anal. Calcd. for C₃₆H₅₅AgF₃N₆O₄PS (863.76 g/mol): C, 50.06; H, 6.42; N, 9.73. Found: C, 48.86; H, 5.82; N, 10.30.

 $[(^3PDAl_2)Ag_2(PPh_3)_2][OTf]_2$ **Synthesis** of $([Ag_2(PPh_3)_2][OTf]_2)$. $\{[Ag_2(NCMe)][OTf]_2\}_n$ (49.3 mg, 0.049 mmol) was dispersed in 6 mL of THF. PPh3 (26.9 mg, 0.102 mmol) was added as a solid. The reaction mixture was stirred at room temperature for 1 h, during which time the solution turned to a pale golden-yellow color. The mixture was then filtered through Celite, and the filtrate was layered with 12 mL n-hexane. Storage of the system at room temperature for 3 d afforded [Ag₂(PPh₃)₂][OTf]₂ as colorless blocks. Yield: 53.2 mg (73 %). ¹H NMR (600 MHz, CD₃CN, 25 °C): δ = 8.37 (s, 4H, CH=N), 7.94 (s, 4H, py m-H), 7.49 (t, ${}^{3}J_{HH}$ = 7.4 Hz, 6H, PPh₃ p-H), 7.39 (t, ${}^{3}J_{HH}$ = 7.4Hz, 12H, PPh₃ m-H), 7.28 (t, $^{3}J_{HH}$ = 7.7 Hz, 12H, PPh₃ o-H), 3.77 (br s, 8H, $CH_2CH_2CH_2$), 2.15 (br s, 4H, $CH_2CH_2CH_2$), 1.37 (s, 18H, C(C H_3)₃) ppm. ¹³C{¹H} NMR (151 MHz, CD₃CN, 25 °C): δ = 165.05 (s, py C), 162.94 (s, CH=N), 153.16 (s, py C), 134.41 (d, $^{2}J_{PC}$ = 16.2 Hz, Ph o-C), 132.40 (d, $^{1}J_{PC}$ = 30.3 Hz, P-C), 131.88 (s, Ph p-C), 130.22 (d, ${}^{3}J_{PC}$ = 9.3 Hz, Ph m-C), 124.73 (s, py m-C), 122.20 (q, ${}^{1}J_{FC}$ = 321.1 Hz, CF₃SO₃), 60.83 (s, CH₂CH₂CH₂), 36.10 (s, C(CH₃)₃), 30.50 (s, C(CH₃)₃), 30.27 (s, CH₂CH₂CH₂) ppm. $^{31}P\{^{1}H\}$ NMR (162 MHz, CD₃CN, 25 °C): δ = -9.73 (br s, *P*Ph₃) ppm. ¹⁹F{¹H} NMR (376 MHz, CD₃CN, 25 °C): δ = -79.34 (s, CF_3SO_3) ppm. Anal. Calcd. for $C_{66}H_{68}Ag_2F_6N_6O_6P_2S_2$ (1497.10 g/mol): C, 52.95; H, 4.58; N, 5.61. Found: C, 53.41; H, 4.46; N, 5.28

Synthesis of $[(^3PDAl_2)Ag_2(CNxyl)_2][OTf]_2$ ($[Ag_2(CNxyl)_2][OTf]_2$). { $[Ag_2(NCMe)][OTf]_2$ }_n (82.0 mg, 0.081 mmol) was dispersed in 6 mL of THF. 2,6-dimethylphenyl isocyanide (21.2 mg, 0.162 mmol) was added as a solid. The reaction mixture was stirred at room temperature for 2 h, during which time the solution became pale golden-yellow in color. The

solution was filtered, and the filtrate was layered with 12 mL nhexane. Storage of the system at room temperature for 6 d yielded [Ag2(CNxyI)2][OTf]2·0.5 THF·0.5 (n-hexane) as golden yellow needles. Yield: 55.2 mg (52 %). ¹H NMR (600 MHz, CD₃CN, 25 °C): δ = 8.36 (s, 4H, CH=N), 7.58 (s, 4H, py m-H), 7.30 (t, ${}^{3}J_{HH}$ = 7.6 Hz, 2H, Ar p-H), 7.16 (d, ${}^{3}J_{HH}$ = 7.7 Hz, 4H, Ar m-H), 4.06 (br s, 8H, CH₂CH₂CH₂), 2.68 (br s, 4H, CH₂CH₂CH₂), 2.40 (s, 12H, $ArCH_3$), 1.25 (s, 18H, $C(CH_3)_3$) ppm. ¹³ $C\{^1H\}$ NMR (151 MHz, CD₃CN, 25 °C): δ = 166.51 (s, py *p-C*), 160.84 (s, *CH*=N), 149.95 (s, Ar C), 152.41 (br s, C≡N) 150.37 (s, py o-C), 136.76 (s, Ar o-C), 131.84 (s, Ar p-C), 129.29 (s, Ar m-C), 126.53 (s, py m-C), 125.76 (br s, C–NC), 122.20 (q, ${}^{1}J_{FC}$ = 321.3 Hz, $CF_{3}SO_{3}$), 61.68 (s, CH₂CH₂CH₂), 36.14 (s, C(CH₃)₃), 30.44 (s, C(CH₃)₃), 30.37 (s, CH₂CH₂CH₂), 18.93 (s, ArCH₃) ppm. Anal. Calcd. for $C_{48}H_{56}Ag_2F_6N_8O_6S_2$ (1234.87 g/mol): C, 46.69; H, 4.57; N, 9.07. Found: C, 46.03; H, 4.36; N, 8.89.

Supporting Information

The supporting information is available free of charge and includes NMR spectroscopic data, crystallographic data, and additional computational details. Deposition Number(s) <url href="https://www.ccdc.cam.ac.uk/services/structures?id=doi :10.1002/###.20220XXX"> 2266461 (for $[Aq_2(CNxyI)_2][OTf]_2 \cdot 0.5 THF \cdot 0.5 (n-hexane), 2266462$ (for [Ag₂(PPh₃)₂][OTf]₂), 2266463 (for [Ag][OTf]·0.5 THF), [Ag(BPh₄)]), 2266464 (for 2266465 (for $\{[Ag_2(NCMe)][OTf]_2\}_n\}$ and 2266466 (for [Ag(PMe₃)][OTf]·THF)</url> contain(s) the supplementary crystallographic data for this paper. These data can be obtained free of charge by the joint Cambridge Crystallographic Data Centre and Fachinformationszentrum Karlsruhe <url

href="http://www.ccdc.cam.ac.uk/structures">Access Structures service</url>.

Acknowledgements

The research was supported by the University of Pennsylvania and by the National Science Foundation's Division of Chemistry (CHE-1945265).

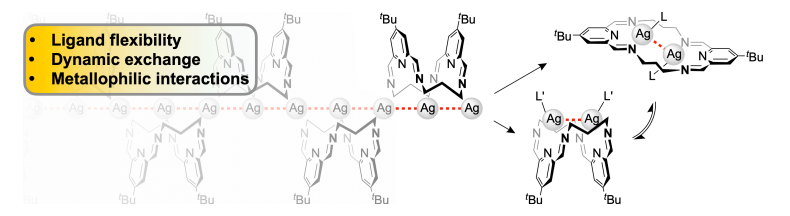
Keywords: metallophilic interactions • disilver complexes • multi-nuclearity • macrocycles • QTAIM

- [1] aD. J. Shields, T. Elkoush, E. Miura-Stempel, C. L. Mak, G.-H. Niu, A. D. Gudmundsdottir, M. G. Campbell, *Inorg. Chem.* 2020, 59, 18338-18344; bE. M. Njogu, B. Omondi, V. O. Nyamori, *J. Coord. Chem.* 2015, 68, 3389-3431.
- [2] A. Kascatan-Nebioglu, M. J. Panzner, C. A. Tessier, C. L. Cannon, W. J. Youngs, Coord. Chem. Rev. 2007, 251, 884-895.
- [3] aA. C. Lane, M. V. Vollmer, C. H. Laber, D. Y. Melgarejo, G. M. Chiarella, J. P. Fackler, X. Yang, G. A. Baker, J. R. Walensky, *Inorg. Chem.* 2014, 53, 11357-11366; bS.-P. Luo, J.-M. Lei, S.-Z. Zhan, *J. Coord. Chem.* 2018, 71, 1193-1204.
- [4] M. Jansen, Angew. Chem. Int. Ed. Engl. 1987, 26, 1098-1110.

- [5] aP. K. Mehrotra, R. Hoffmann, *Inorg. Chem.* 1978, 17, 2187-2189; bP. Pyykkö, *Chem. Rev.* 1997, 97, 597-636; cS. Grimme, J.-P. Djukic, *Inorg. Chem.* 2011, 50, 2619-2628; dM. Andrejić, R. A. Mata, *Phys. Chem. Chem. Phys.* 2013, 15, 18115-18122; eQ. Wan, J. Yang, W.-P. To, C.-M. Che, *Proc. Natl. Acad. Sci. U.S.A.* 2021, 118, e2019265118.
- [6] aS. Raju, H. B. Singh, R. J. Butcher, *Dalton Trans.* 2020, 49, 9099-9117; bA. Vellé, L. Rodríguez-Santiago, M. Sodupe, P. J. Sanz Miguel, *Chem. Eur. J.* 2020, 26, 997-1002; cA. S. Novikov, *Inorg. Chim. Acta* 2018, 483, 21-25.
- [7] P. Pyykkö, N. Runeberg, F. Mendizabal, Chem. Eur. J. 1997, 3, 1451-1457.
- [8] aH. Schmidbaur, A. Schier, Angew. Chem. Int. Ed.
 2015, 54, 746-784; bB. Berti, M. Bortoluzzi, C. Cesari,
 C. Femoni, M. C. Iapalucci, R. Mazzoni, F. Vacca, S.
 Zacchini, Inorg. Chem. 2019, 58, 2911-2915; cL. H.
 Doerrer, Comment. Inorg. Chem. 2008, 29, 93-127.
- [9] aA. K. Jassal, *Inorg. Chem. Front.* 2020, 7, 3735-3764; bY.-P. Xie, J.-L. Jin, G.-X. Duan, X. Lu, T. C. W. Mak, *Coord. Chem. Rev.* 2017, 331, 54-72.
- [10] aS. Joardar, S. Roy, S. Samanta, A. Kumar Dutta, J. Chem. Sci. 2015, 127, 1819-1826; bR. A. Evarestov, A. I. Panin, Y. S. Tverjanovich, J. Comput. Chem. 2021, 42, 242-247; cJ. Moussa, L. M. Chamoreau, M. P. Gullo, A. Degli Esposti, A. Barbieri, H. Amouri, Dalton Trans. 2016, 45, 2906-2913; dS. Ahmad, M. Hanif, M. Monim-ul-Mehboob, A. A. Isab, M. A. Alotaibi, T. Ahmad, Polyhedron 2022, 214, 115643.
- aL. Ray, M. M. Shaikh, P. Ghosh, *Inorg. Chem.* 2008, 47, 230-240; bE. O'Grady, N. Kaltsoyannis, *Phys. Chem. Chem. Phys.* 2004, 6, 680-687; cL. Magnko, M. Schweizer, G. Rauhut, M. Schütz, H. Stoll, H.-J. Werner, *Phys. Chem. Chem. Phys.* 2002, 4, 1006-1013; dJ. Zheng, Z. Lu, K. Wu, G.-H. Ning, D. Li, *Chem. Rev.* 2020, 120, 9675-9742; eA. Caballero-Muñoz, J. M. Guevara-Vela, A. Fernández-Alarcón, M. A. Valentín-Rodríguez, M. Flores-Álamo, T. Rocha-Rinza, H. Torrens, G. Moreno-Alcántar, *Eur. J. Inorg. Chem.* 2021, 2021, 2702-2711.
- [12] aP. Cui, Q. Wang, S. P. McCollom, B. C. Manor, P. J. Carroll, N. C. Tomson, Angew. Chem. Int. Ed. 2017, 56, 15979-15983; bA. Z. Spentzos, M. R. Gau, P. J. Carroll, N. C. Tomson, Chem. Commun. 2020, 56, 9675-9678; cT. Liu, M. R. Gau, N. C. Tomson, J. Am. Chem. Soc. **2020**, 142, 8142-8146; dQ. Wang, S. Zhang, P. Cui, A. B. Weberg, L. M. Thierer, B. C. Manor, M. R. Gau, P. J. Carroll, N. C. Tomson, Inorg. Chem. 2020, 59, 4200-4214; eS. Zhang, Q. Wang, L. M. Thierer, A. B. Weberg, M. R. Gau, P. J. Carroll, N. C. Tomson, Inorg. Chem. 2019, 58, 12234-12244; fS. Zhang, P. Cui, T. Liu, Q. Wang, T. J. Longo, L. M. Thierer, B. C. Manor, M. R. Gau, P. J. Carroll, G. C. Papaefthymiou, N. C. Tomson, Angew. Chem. Int. Ed. 2020, 59, 15215-15219; gL. M. Thierer, Q. Wang, S. H. Brooks, P. Cui, J. Qi, M. R. Gau, B. C. Manor, P. J. Carroll, N. C. Tomson, Polyhedron 2021, 198, 115044. Attempts to make Ag-containing complexes bearing [13]
- [13] Attempts to make Ag-containing complexes bearing the ketimine-based analogs of this ligand resulted in intractable mixtures of products.
 [14] aM. J. Hannon, C. L. Painting, E. A. Plummer, L. J.
- Childs, N. W. Alcock, *Chem. Eur. J.* **2002**, *8*, 2225-2238; bK. Xiong, M. Wu, Q. Zhang, W. Wei, M. Yang, F. Jiang, M. Hong, *Chem. Commun.* **2009**, 1840-1842.
- [15] A. G. Young, L. R. Hanton, Coord. Chem. Rev. 2008, 252, 1346-1386.
- [16] aR.-L. Sang, L. Xu, Eur. J. Inorg. Chem. 2006, 2006, 1260-1267; bl. Capel Berdiell, S. L. Warriner, M. A. Halcrow, Dalton Trans. 2018, 47, 5269-5278.
- [17] S. Alvarez, Dalton Trans. 2013, 42, 8617-8636.
- [18] C. Römelt, T. Weyhermüller, K. Wieghardt, *Coord. Chem. Rev.* **2019**, *380*, 287-317.
- [19] C. R. Groom, I. J. Bruno, M. P. Lightfoot, S. C. Ward, Acta Crystallogr. B 2016, 72, 171-179.

- [20] F. A. Cotton, Acc. Chem. Res. 1978, 11, 225-232.
- [21] L. Yang, D. R. Powell, R. P. Houser, *Dalton Trans.* **2007**, 955-964.
- [22] C. R. Martinez, B. L. Iverson, Chem. Sci. 2012, 3, 2191-2201.
- [23] aÉ. Fournier, F. Lebrun, M. Drouin, A. Decken, P. D. Harvey, *Inorg. Chem.* 2004, 43, 3127-3135; bB. Djordjevic, O. Schuster, H. Schmidbaur, *Inorg. Chem.* 2005, 44, 673-676.
- [24] A. Otero-de-la-Roza, J. D. Mallory, E. R. Johnson, J. Chem. Phys. 2014, 140, 18A504.
- [25] aL. Zhao, M. von Hopffgarten, D. M. Andrada, G. Frenking, WIREs Comput. Mol. Sci. 2018, 8, e1345; bQ. Zheng, S. Borsley, G. S. Nichol, F. Duarte, S. L. Cockroft, Angew. Chem. Int. Ed. 2019, 58, 12617-12623.
- [26] aR. F. W. Bader, Acc. Chem. Res. 1985, 18, 9-15; bC. Lepetit, P. Fau, K. Fajerwerg, M. L. Kahn, B. Silvi, Coord. Chem. Rev. 2017, 345, 150-181.
- [27] P. Popelier, *Atoms in Molecules: An Introduction*, Pearson Education Limited, Edinburgh Gate, Harlow, **2000**.
- [28] R. Bianchi, G. Gervasio, D. Marabello, *Inorg. Chem.* **2000**, *39*, 2360-2366.
- [29] Similar analyses (QTAIM, MBO and IBSI) were also performed on {[Ag2(NCMe)][OTf]2}n, in which the molecule being analysed contains two [(3PDAI2)Ag(NCMe)][Ag]²⁺ units. The results, presented in Table S4 of the Electronic Supporting Information, are consistent with weak metallophilic interactions between the Ag centers.
- [30] aT. Lu, Q. Chen, J. Comput. Chem. 2022, 43, 539-555;
 bC. Lefebvre, G. Rubez, H. Khartabil, J.-C. Boisson, J. Contreras-García, E. Hénon, Phys. Chem. Chem. Phys. 2017, 19, 17928-17936.
- [31] J. Klein, H. Khartabil, J.-C. Boisson, J. Contreras-García, J.-P. Piquemal, E. Hénon, J. Phys. Chem. A 2020, 124, 1850-1860.
- [32] B. Pinter, L. Broeckaert, J. Turek, A. Růžička, F. De Proft. Chem. Eur. J. 2014, 20, 734-744.
- [33] B. Assadollahzadeh, P. Schwerdtfeger, *Chem. Phys. Lett.* **2008**, *462*, 222-228.
- [34] M. L. Luetkens Jr., A. P. Sattelberger, H. H. Murray, J. D. Basil, J. P. Fackler Jr., R. A. Jones, D. E. Heaton, in *Inorganic Syntheses*, 1989, pp. 7-12.
- [35] W. L. F. Armarego, C. Chai, *Purification of organic chemicals*, 6th ed., Butterworth-Heinemann, Oxford, 2009
- [36] F. Neese, WIREs Comput. Mol. Sci. 2012, 2, 73-78.
- [37] aS. Grimme, *J. Comput. Chem.* **2006**, 27, 1787-1799; bS. Grimme, J. Antony, S. Ehrlich, H. Krieg, *J. Chem. Phys.* **2010**, *132*, 154104-154101-154119; cS. Grimme, S. Ehrlich, L. Goerigk, *J. Comput. Chem.* **2011**, *32*, 1456-1465.
- [38] aA. Schäfer, H. Horn, R. Ahlrichs, J. Chem. Phys. 1992, 97, 2571-2577; bD. A. Pantazis, X.-Y. Chen, C. R. Landis, F. Neese, J. Chem. Theory Comput. 2008, 4, 908-919; cA. Schäfer, C. Huber, R. Ahlrichs, J. Chem. Phys. 1994, 100, 5829-5835; dF. Weigend, R. Ahlrichs, Phys. Chem. Chem. Phys. 2005, 7, 3297-3305
- [39] E. F. Pettersen, T. D. Goddard, C. C. Huang, G. S. Couch, D. M. Greenblatt, E. C. Meng, T. E. Ferrin, J. Comput. Chem. 2004, 25, 1605-1612.
- [40] T. Lu, F. Chen, J. Comput. Chem. 2012, 33, 580-592.
- [41] W. Humphrey, A. Dalke, K. Schulten, J. Mol. Graph. 1996, 14, 33-38.
- [42] SAINT, v8.38A, Bruker AXS Inc., Madison, WI, 2014.
- [43] *CrysAlisPro 1.171.40.89a*, Rigaku Oxford Diffraction, Rigaku Corporation, Oxford, UK, **2020**.
- [44] L. Krause, R. Herbst-Irmer, G. M. Sheldrick, D. Stalke, J. Appl. Crystallogr. 2015, 48, 3-10.
- [45] SCALE3 ABSPACK: an Oxford Diffraction program, v1.0.7, Oxford Diffraction Ltd., Abingdon, UK, 2005.
- [46] G. Sheldrick, Acta Crystallogr. A 2015, 71, 3-8.

Entry for the Table of Contents



A flexible macrocyclic ligand is used to support the synthesis of diargentous complexes with varying geometries of Ag^I – Ag^I interactions. Spectroscopic studies indicate that the Ag_2 systems retain both Ag ions during dramatic geometric changes in solution. A computational study indicated that non-covalent, inter-ligand – not metallophilic – interactions contribute to the observed solid-state geometries.

